

Article

Pt-Based Electrocatalyst Modified by CsH₂PO₄/SiP₂O₇ for Electrochemical Oxidation of NH₃ to H₂ in Solid Acid Electrolysis Cell

Jihoon Kim ^{1,†}, Daehee Jang ^{1,†}, Junil Choi ¹, Junbeom Maeng ¹, Hyun Ho Shin ¹, Taiho Park ¹
and Won Bae Kim ^{1,2,*}

¹ Department of Chemical Engineering, Pohang University of Science and Technology (POSTECH), 77 Cheongam-ro, Nam-gu, Pohang 37673, Gyeongbuk, Republic of Korea

² Graduate Institute of Ferrous & Energy Materials Technology, Pohang University of Science and Technology (POSTECH), 77 Cheongam-ro, Nam-gu, Pohang 37673, Gyeongbuk, Republic of Korea

* Correspondence: kimwb@postech.ac.kr; Tel.: 82-54-279-2397; Fax: 82-54-279-5528

† These authors contributed equally to this work.

Abstract: Ammonia (NH₃) has received much attention as a hydrogen carrier because it can be easily liquefied with a high hydrogen storage density and emits no greenhouse gas during the dihydrogen evolution process. The ammonia oxidation reaction (AOR) in an electrochemical system has an important merit in which a very high-purity dihydrogen gas can be obtained without an additional separation process that is typically needed for thermochemical decomposition processes. Herein, the electrochemical AOR was carried out in a solid acid electrolysis cell (SAEC) at an intermediate temperature around 250 °C, in which a solid composite of CsH₂PO₄ mixed with SiP₂O₇ was used as an electrolyte and Pt/C-based electrocatalysts were employed as the electrode materials of both anode and cathode. The Pt/C electrode material was modified with the CsH₂PO₄/SiP₂O₇ electrolyte in order to enhance the electrocatalytic activity for the AOR with an improved H₂ production rate. Over the SAEC system reported here, a high AOR performance was obtained with a current density of 67.1 mA/cm² and Faradaic efficiency (FE) of 98.2%. This study can suggest the significant potential of SAEC for the carbon-free H₂ production from the selective electrochemical oxidation of NH₃.

Keywords: ammonia oxidation; solid acid electrolysis cell; electrocatalysis; green hydrogen; CsH₂PO₄/SiP₂O₇



Citation: Kim, J.; Jang, D.; Choi, J.; Maeng, J.; Shin, H.H.; Park, T.; Kim, W.B. Pt-Based Electrocatalyst Modified by CsH₂PO₄/SiP₂O₇ for Electrochemical Oxidation of NH₃ to H₂ in Solid Acid Electrolysis Cell. *Catalysts* **2023**, *13*, 707. <https://doi.org/10.3390/catal13040707>

Academic Editor: Barbara Mecheri

Received: 28 February 2023

Revised: 4 April 2023

Accepted: 4 April 2023

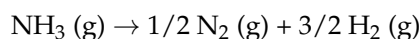
Published: 6 April 2023



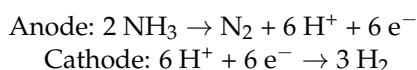
Copyright: © 2023 by the authors. Licensee MDPI, Basel, Switzerland. This article is an open access article distributed under the terms and conditions of the Creative Commons Attribution (CC BY) license (<https://creativecommons.org/licenses/by/4.0/>).

1. Introduction

The increasing environmental hazards from global warming have triggered extensive research for alternative energy sources to the conventional fossil fuels [1,2]. Dihydrogen (H₂) gas has been suggested as the favorable, alternative energy carrier since H₂ has a high gravimetric energy density and the only product from its use is clean water. However, the storage and transport of H₂ suffers from its low volumetric energy density, necessitating complicated equipment for extreme conditions of temperature and pressure for liquid-state H₂ [3]. Therefore, various materials, such as liquid organic hydrogen carriers (LOHC), metal hydrides, and ammonia, have been studied for use as an H₂ carrier. Among them, ammonia (NH₃) has received great attention as an H₂ gas carrier material recently due to its high volumetric density of hydrogen, easy liquefaction and storage conditions (−33 °C or 8 bar at ambient temperature), no greenhouse gas emission during decomposition, and the presence of existing infrastructure in the current society [4–6]. H₂ evolution from ammonia can be simply performed via a thermal decomposition process described by the following reaction:



As ammonia decomposition is favored at high temperatures, this thermal decomposition of ammonia generally requires more than 400 °C to achieve high conversion. Moreover, an additional separation process to obtain a pure dihydrogen gas is necessary because unconverted NH₃ from the thermal decomposition process can damage hydrogen application systems [7]. Therefore, thermal decomposition of NH₃ to H₂ requires high energy, and thus an alternative H₂ evolution process from NH₃ needs to be developed. Recently, alternative methods of electrolysis processes have been studied to produce high-purity dihydrogen from the electrochemical oxidation of liquid phase ammonia. The electrochemical ammonia oxidation reaction (AOR) for dihydrogen evolution involves following half-cell reactions of oxidation and reduction processes at the anode and cathode, respectively:



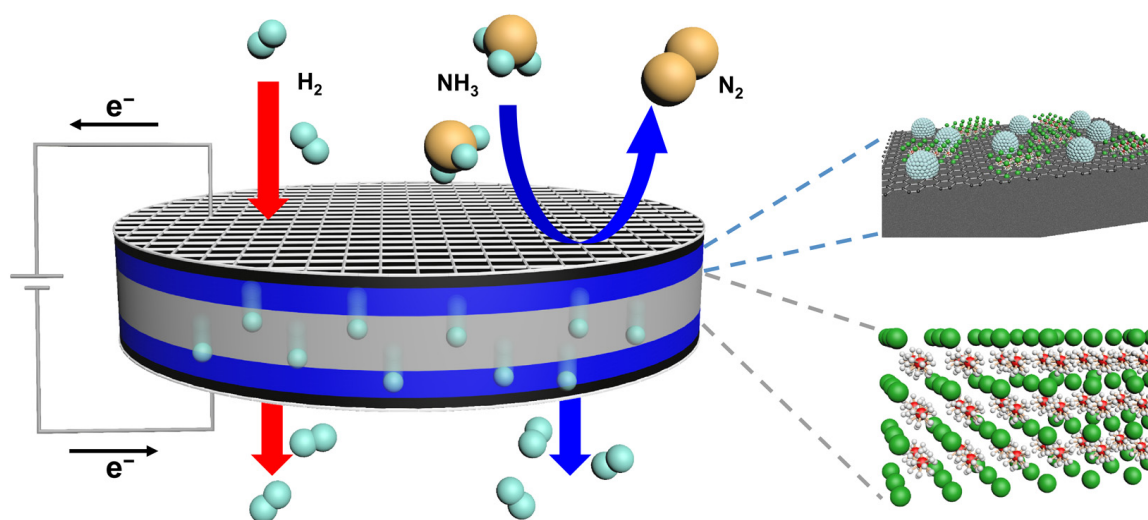
The AOR is performed over the electrolysis cells that are fabricated by membrane electrolytes sandwiched with anode and cathode electrodes. Thereby, a high-purity dihydrogen gas can be produced at the cathode side under ambient conditions [8–10]. Despite this advantage, however, the AOR under ambient condition is still to be improved significantly in terms of the H₂ production rate as compared to the thermal decomposition processes. The solid acid electrolysis cell (SAEC), which can operate at intermediate temperature ranges from 200 °C to 300 °C, has attracted its uses for electrochemical oxidation/reduction processes by circumventing some limitations of low temperature electrolysis cells. Solid acid compounds, which are charge-balanced with SO₄²⁻ and PO₄³⁻ oxyanions, can be used as an excellent proton-conducting electrolyte for SAECs due to their phase transition properties to superprotonic phases even at the relatively low and intermediate temperatures with high proton conductivities [11]. Among them, cesium dihydrogen phosphate (CsH₂PO₄) is a representative solid acid, which reveals a high proton conductivity at 250 °C and has a relatively high tolerance against NH₃ [12,13]. This CsH₂PO₄ is transformed to a superprotonic phase at about 228 °C and exhibits a high proton conductivity of 10⁻² S cm⁻¹ or greater [14]. In addition, a humidified environment is typically required in order to prevent dehydration and dissociation of CsH₂PO₄. The CsH₂PO₄ electrolyte has another issue to be resolved: it suffers from a relatively low mechanical stability, hence several studies about binder additives have been performed for SAEC systems [15–17].

Recently, to overcome the limitations of both thermal and electrochemical ammonia decomposition, a hybrid type of thermal-electrochemical ammonia conversion using an SAEC has been proposed. Lim et al. [18] demonstrated a hybrid system of thermal decomposition of ammonia followed by electrochemical dihydrogen production at 250 °C using CsH₂PO₄ as a proton-conducting electrolyte. This result showed a similar level of high H₂ production rates to the studies in the temperature range from 350 to 500 °C, but the high loading weight of Ru catalyst (>10 mg_{Ru} cm⁻²) was required for the ammonia thermal decomposition part. Moreover, an additional Pt electrocatalyst layer for hydrogen oxidation is required for the system. In this sense, developing an efficient electrolyte and lowering the noble metal use are effective and necessary approaches for AOR research using SAEC systems.

In this study, we report the electrochemical AOR using the SAEC system at intermediate temperature to produce high-purity dihydrogen gas with a high production rate. For the enhanced mechanical properties and high proton conductivity in the relatively broad temperature range, the CsH₂PO₄ electrolyte was composited with a silica-based material of SiP₂O₇. As CsH₂PO₄ and SiP₂O₇ can react to form CsH₅(PO₄)₂ under a hydrothermal condition, the electrolyte provides high proton conductivity in a temperature range from 150 °C to 280 °C [13]. Moreover, Pt/C-based electrocatalyst was blended with the electrolyte composite for a high-performance SAEC to produce H₂ from the electrochemical oxidation of NH₃. A high rate of 1.33 mmol cm⁻² h⁻¹ and faradaic efficiency (FE) of 98.2% for the H₂ production were achieved in the SAEC system reported here.

2. Results and Discussion

Scheme 1 illustrates the SAEC cell configuration used in this study. The cell was composed of a stainless steel mesh current collector, electrodes of anode and cathode with electrocatalysts on carbon paper, and a solid-state electrolyte. The electrolyte was prepared by mixing the synthesized CsH_2PO_4 (CDP) and SiP_2O_7 (SPO) in a 1:2 molar ratio, which is described in detail in the experimental section. The electrolyte composite and Pt/C catalyst were blended in a series of weight ratios to use as electrode materials and deposited on the carbon paper (Pt/C_CDP/SPO- x , $x = 3, 6, 9$). The morphology and crystal structure of the electrode materials were investigated by scanning electron microscopy (SEM) and X-ray diffraction (XRD), respectively, to check the fabrication procedure of the electrode paper. The formation of CsH_2PO_4 and SiP_2O_7 was examined by XRD, as shown in Figure 1a. Compared to the XRD patterns of each material, the composite materials on the electrode paper indicated weak peaks relating to a phase of SPO, because the CDP and SPO likely reacted to form $\text{CsH}_5(\text{PO}_4)_2$ under the hydrothermal condition by the following reaction [13]:



Scheme 1. Schematic illustration of electrocatalytic hydrogen oxidation reaction (HOR) and ammonia oxidation reaction (AOR) in solid acid electrolysis cell (SAEC).

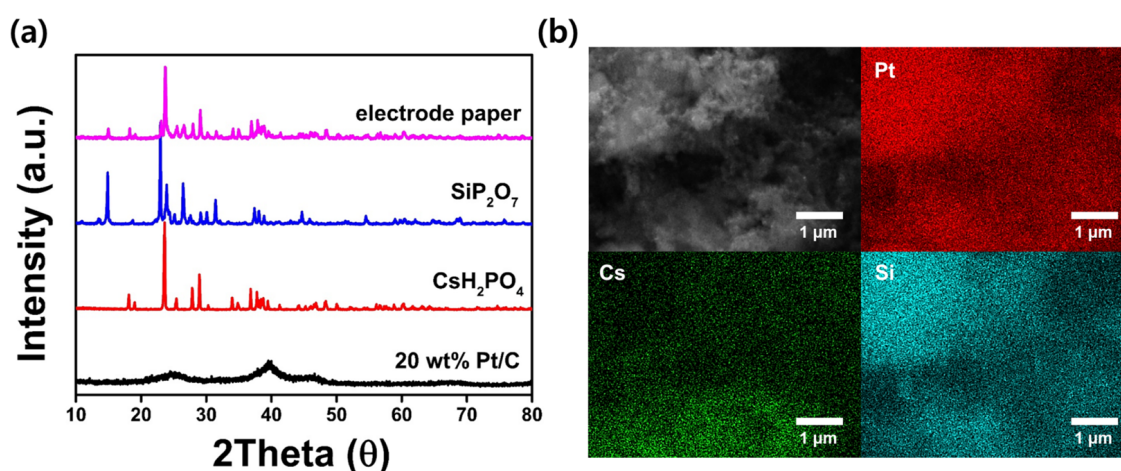


Figure 1. (a) XRD patterns of Pt/C, CDP, SPO, and electrode paper. (b) SEM image of electrode material and EDS elemental mapping of Pt, Cs, and Si.

However, the XRD peak at around 40° of Pt (111) was not detected clearly in the electrode paper because the intensities of XRD peaks referring to the CDP and SPO were much stronger due to the high crystalline properties of CDP and SPO. To investigate the mixing of the Pt/C and electrolyte composite, elemental mappings were carried out in the SEM image, indicating that Pt, Cs, and Si were uniformly dispersed over the electrode surface (Figure 1b). The XRD and SEM results showed that the Pt/C and electrolyte composite were nicely mixed and uniformly deposited on the carbon paper.

To interpret the proton-conducting properties of the CDP/SPO electrolyte, the current density and faradaic efficiency (FE) of dihydrogen evolution reaction were measured. CDP is known in that it can reveal a high proton conductivity in the range of 220°C to 270°C by accompanying the phase transition from a monoclinic crystal structure to superprotonic cubic structure over a temperature of 220°C . Proton conductivity values of CDP and CDP/SPO were estimated by fitting the electrochemical impedance spectroscopy (EIS) data, especially those obtained at high frequency ranges. The proton conductivity values were obtained every 10°C from 160°C to 250°C (Figure 2a). The CDP alone exhibited a high proton conductivity at the temperature of 220°C , which is in a good agreement with its phase transition feature, but the CDP/SPO showed no sharp decline of proton conductivity below 220°C [19]. Moreover, the proton conductivity value of CDP/SPO was higher than that of CDP at 250°C . This indicated that the addition of SPO into CDP could enhance thermal stability as well as proton conductivity of the electrolyte. Using the CDP/SPO as a composited electrolyte, the linear sweep voltammetry (LSV) of hydrogen oxidation reaction (HOR) at 250°C indicated that the current density increased linearly as the applied voltage increased (Figure 2b), and the FE of H_2 evolution was reached around 100%. These results revealed that the CDP/SPO electrolyte can perform with a great proton conductivity at 250°C .

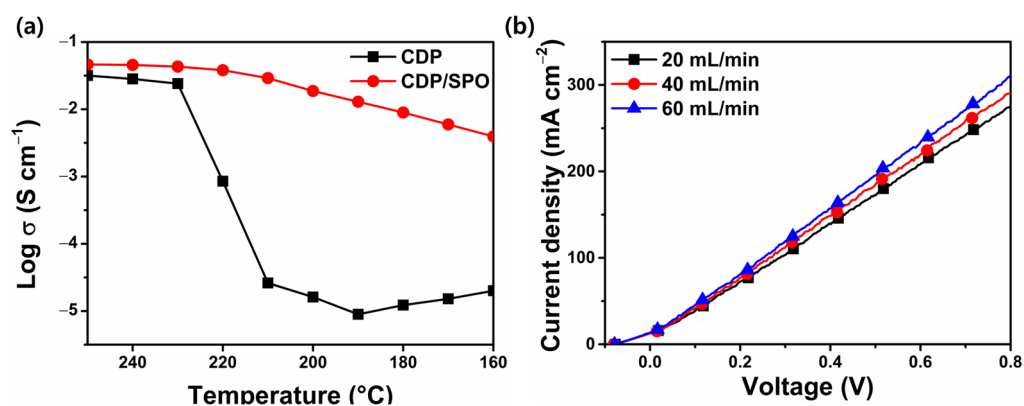


Figure 2. (a) Conductivity values of CDP and CDP/SPO from 160°C to 250°C . (b) LSV curves of HOR using CDP/SPO electrolyte at different hydrogen flow rate.

A series of Pt/C_CDP/SPO electrodes was applied for the AOR over the SAEC system to optimize the weight ratios of Pt/C and electrolyte composite. The linear sweep voltammetry (LSV) curves of the catalysts at 10 mV s^{-1} scan rate were investigated from 0 V to 0.8 V (Figure S1). The LSV curves showed the increased slopes of current density versus voltage after 0.4 V , indicating that the AOR should occur faster from 0.4 V . Figure 3a indicates the measured current density for the AOR at $0.5\text{--}0.8\text{ V}$ using the Pt/C and Pt/C_CDP/SPO- x catalysts. Pt/C_CDP/SPO-6, which is the mixture of Pt/C and electrolyte composite in a 1:6 weight ratio, showed the best current density compared to the Pt/C, without compositing CDP/SPO or Pt/C_CDP/SPO with other ratio mixtures. EIS data were analyzed to find further insight into the charge transfer kinetics of Pt/C_CDP/SPO- x catalysts for the AOR in the SAEC. The EIS measurement was carried out at an open circuit voltage under 60 mL min^{-1} ammonia flow rate condition. Figure 3b shows the Nyquist plots of Pt/C_CDP/SPO- x catalysts; the electrochemical impedance parameters were evaluated using the equivalent circuit model shown in the inset of Figure 3b. The equivalent circuit

consists of one ohmic resistance (R_s), inductance (L_1), and two parallel circuits of constant phase element (CPE_1 , CPE_2) and non-ohmic polarization resistance (R_1 , R_2) [15]. The fitted data were summarized in Table S1. L_1 was invariant for the catalysts because it is attributed to the inductance of the cables used in the impedance measurement device. As shown in Figure 3b, the Nyquist plots show that the high-frequency x -axis intercepts of Pt/C_CDP/SPO- x catalysts, which are mainly attributed to the ohmic resistance associated with the interfacial resistance between electrolyte and electrode, are nearly constant. R_1 and R_2 are the polarization resistance at high frequency range and medium–low frequency range, respectively. R_1 is contributed by the charge transfer resistance at the electrolyte and electrode interface, and R_2 is associated with the chemisorption of reactant and gas transport limitation at the electrode [20]. According to the fitted data, R_1 decreased as the mixed CDP/SPO ratio increased, indicating that mixing the electrolyte composite to Pt/C could improve the charge transfer kinetics in the AOR. However, the R_2 value of Pt/C_CDP/SPO-9 (12.47 Ω) highly increased compared to the Pt/C_CDP/SPO-3 (9.59 Ω) and Pt/C_CDP/SPO-6 (9.36 Ω). This might be attributed to the excessive electrolyte composite which caused an inhibition of reactant gas transport and chemisorption over the Pt active sites. Both results with current densities and EIS analysis suggest that there is an optimal ratio between the Pt/C and CDP/SPO, and the Pt/C_CDP/SPO-6 could be better for the electron transfer kinetics in the AOR than the Pt/C_CDP/SPO-3 and Pt/C_CDP/SPO-9.

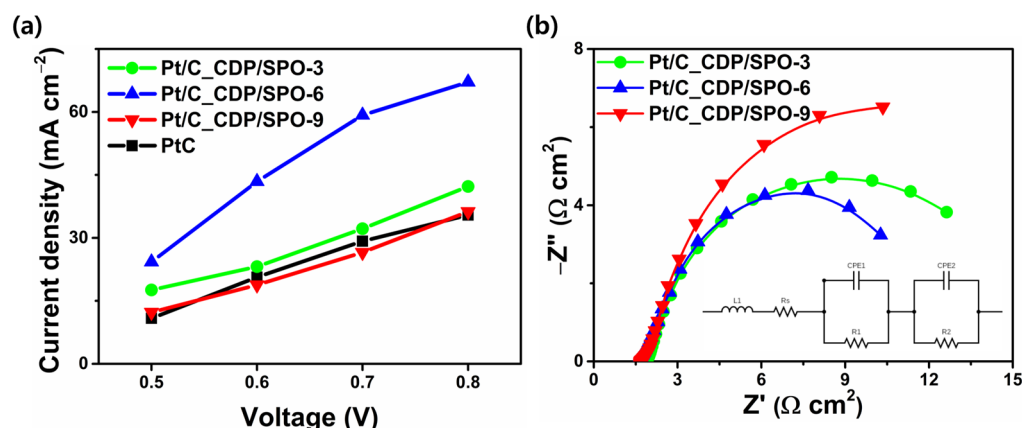


Figure 3. (a) Current density of Pt/C and Pt/C_CDP/SPO- x catalysts at each potential from 0.5 V to 0.8 V. (b) Nyquist plots of Pt/C_CDP/SPO- x catalysts at open circuit voltage; inset shows the equivalent circuit model. Every analysis was performed at 250 °C under NH₃ flow rate of 60 mL min⁻¹.

Using the Pt/C_CDP/SPO-6 catalyst, the AOR in the SAEC was carried out along with different ammonia flow rates of 20, 40, 60 mL min⁻¹. Figure 4 shows that the current densities increased as the voltage and ammonia flow rate were increased. The gas chromatography with thermal conductivity detector (GC-TCD) was operated at every 9 min of reaction time to quantitatively measure the dihydrogen production, and the result is summarized in Table 1. The GC-TCD analysis data of cathode outlet gas at 0.8 V at a flow rate of NH₃ of 60 mL min⁻¹ are illustrated in Figure S2. The GC-TCD chromatogram showed that H₂, N₂, and H₂O were detected at 1.05, 1.15, and 10.5 min, respectively. As humidified N₂ gas was supplied to the cathode, the GC-TCD analysis revealed that only H₂ gas was produced at the cathode. Consequently, FE was 98.2% and H₂ production rate was 1.33 mmol h⁻¹ cm⁻² at an applied potential of 0.8 V at a flow rate of NH₃ of 60 mL min⁻¹, and FE appeared to be decreased as the applied potential was decreased from 0.8 V to 0.5 V. Non-faradaic processes appeared to occur at lower potentials because charge transfer reactions over the electrode would be kinetically unfavorable when the applied potential is not sufficiently high to overcome the overpotentials of AOR [21,22].

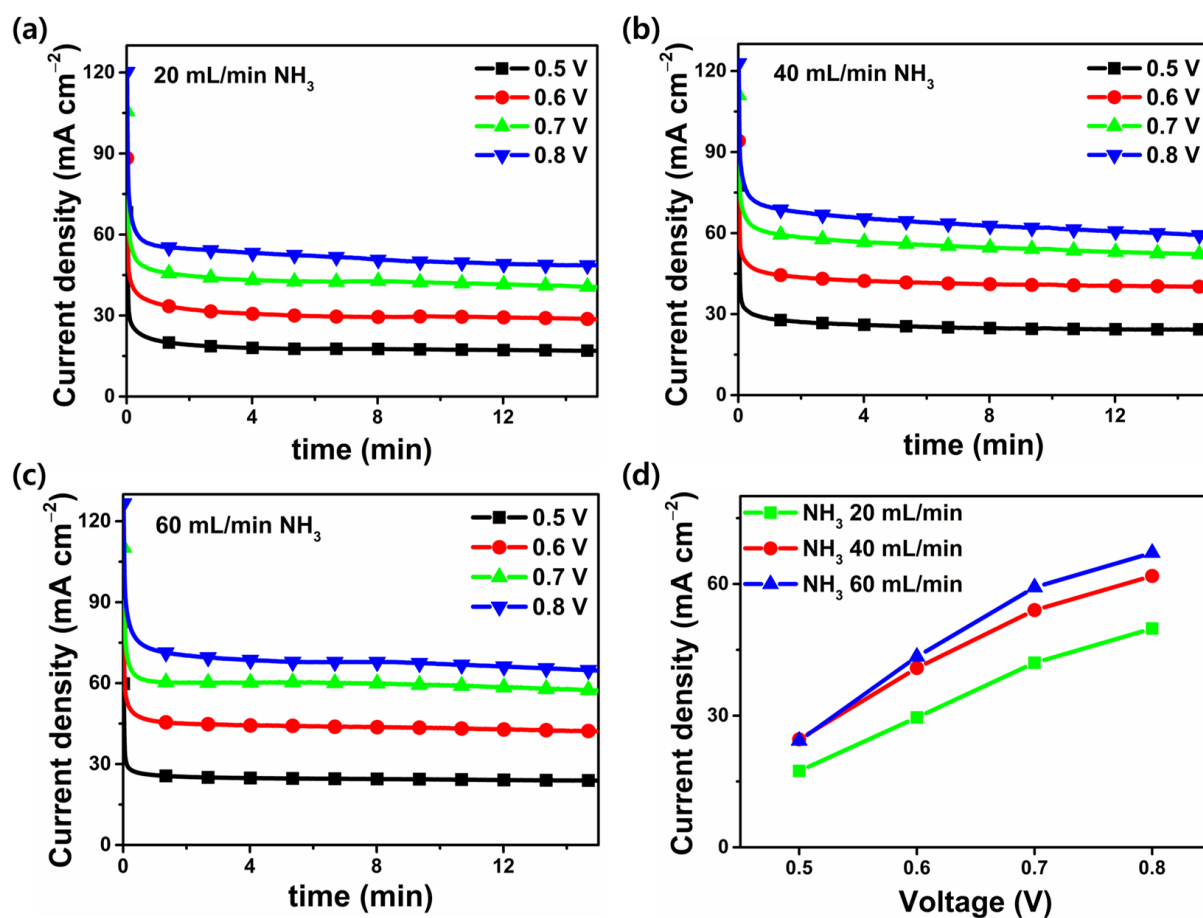


Figure 4. Chronoamperometry tests at potential from 0.5 V to 0.8 V under NH₃ flow rate of (a) 20 mL min⁻¹, (b) 40 mL min⁻¹, and (c) 60 mL min⁻¹. (d) Current density of Pt/C_CDP/SPO-6 catalyst at each potential from 0.5 V to 0.8 V. Every analysis was performed at 250 °C using Pt/C_CDP/SPO-6 catalyst.

Table 1. Summary of AOR results of Pt/C_CDP/SPO-6 at 250 °C.

NH ₃ Flow (mL min ⁻¹)	WHSV (h ⁻¹ Pt)	Voltage (V)	Current Density (mA cm ⁻²)	H ₂ Production Rate (mmol h ⁻¹ cm ⁻²)	Faradic Efficiency (%)
20	183.6	0.5	17.4	0.168	47.9
		0.6	29.6	0.313	52.4
		0.7	42.1	0.480	56.5
		0.8	49.9	0.565	56.1
40	367.2	0.5	24.6	0.312	62.9
		0.6	40.9	0.652	79.0
		0.7	54.0	0.819	75.1
		0.8	61.8	0.982	75.1
60	550.8	0.5	24.3	0.378	76.1
		0.6	43.4	0.745	85.0
		0.7	59.2	1.16	97.0
		0.8	67.1	1.33	98.2

The electrochemical AOR in the SAEC system was carried out for 20 h at an inlet ammonia flow rate of 60 mL min^{-1} at 0.8 V for the long-term durability test of the cell. The corresponding current density profile according to the cell operating time is shown in Figure 5. During the initial 1 h, the ammonia oxidation rate decreased almost linearly, and after 1 h, the current density of 30 mA cm^{-2} was shown. After that, the activity deterioration rate decreased, and the activity of 7.5 mA cm^{-2} was maintained after 8 h. Furthermore, the deactivation rate of the Pt/C_CDP/SPO-6 catalyst during the long-term test was calculated by differentiating chronoamperometric data and illustrated in Figure S3 to investigate the stability of the catalyst [23]. The deactivation rate became lower than $0.015 \text{ mA cm}^{-2} \text{ min}^{-1}$ after 6 h, which signifies that the catalytic activity was maintained with a decline rate of less than 0.1% after 6 h. After the stability test, XRD and SEM analyses of the electrode materials were performed to examine the morphology and crystalline structure of the catalysts. As shown in Figure S4, the XRD pattern of the used electrode material did not change compared to the pristine electrode. If dehydration of CDP took place, the $\text{CsH}_2\text{P}_2\text{O}_7$ and CsPO_3 would be formed, but no peaks referring to the $\text{CsH}_2\text{P}_2\text{O}_7$ and CsPO_3 were detected in the XRD pattern of Pt/C_CDP/SPO-6 measured after the stability test. This XRD result indicated that the Pt/C_CDP/SPO-6 catalyst demonstrates great stability without dehydration of the electrolyte composite. Furthermore, the SEM elemental mapping of Pt, Cs, and Si also showed that the Pt/C and electrolyte composite still dispersed uniformly on the carbon paper. These results indicated that the Pt/C_CDP/SPO-6 catalyst showed highly efficient electrochemical performance with a great stability for the AOR in SAEC.

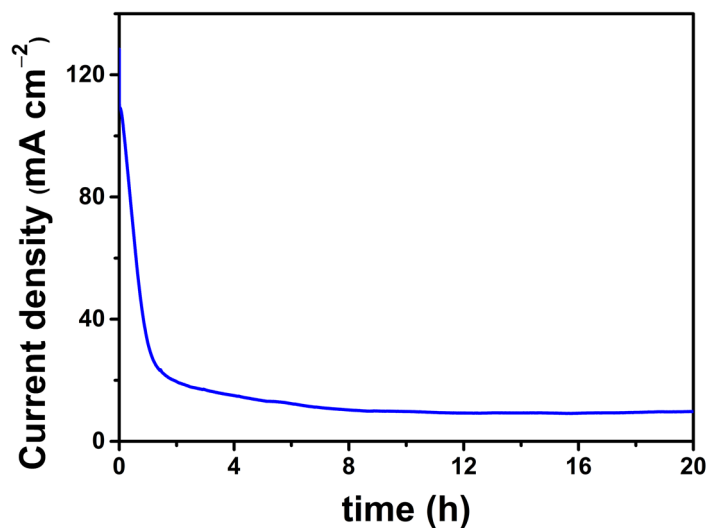


Figure 5. Long-term stability test of Pt/C_CDP/SPO-6 at 0.8 V at NH_3 flow rate of 60 mL min^{-1} for 20 h.

The amount of ammonia crossover that can possibly take place across the electrolyte membrane during the electrochemical AOR was calculated by detecting and quantifying the ammonia dissolved in the water trap via UV-vis spectrophotometry [24,25] using the indophenol blue method (Figure S5). Preventing ammonia crossover is a highly important strategy in this SAEC system since the produced H_2 cannot be used directly in the PEMFC as H_2 fuel if any significant amount of ammonia concentration in the gas is involved [26]. The measured data are summarized in Table S2. The amount of crossed over ammonia collected for 60 min at a cell voltage of 0.8 V was 0.083 micromole , and the partial pressure of crossed ammonia for the outlet gas flow rate of 30 mL min^{-1} would be less than 0.96 ppm . This is under 1 ppm , which is the partial pressure of ammonia that could be accepted for the H_2 feed stream directly into the PEMFC [27]. The residual concentrations of ammonia during the typical thermal decomposition processes are known to be about 1000 ppm or greater, which is definitely subject to the additional separation or removal processes of ammonia to use a pure H_2 , hence the electrochemical AOR process in the SAEC system

proposed here should have a highly significant merit to produce a high-purity H₂ gas from a carbon-free NH₃.

In this work, the Pt/C_CDP/SPO-6 showed a high performance and stability for the electrochemical AOR at intermediate temperatures in the SAEC. Addition of SPO to CDP induced an increase in proton conductivity and an enhancement of thermal stability of the electrolyte, and the charge transfer resistance over the electrode material was further decreased by compositing the Pt/C catalyst with the electrolyte materials. However, excessive addition of CDP/SPO to the Pt/C catalyst appeared to hinder mass transfer and chemisorption of reactant on the active sites; thus, tuning the ratio of electrolyte composite and catalyst materials is significant and will be studied further. As summarized in Figure 6 and Figure S6, the AOR performance in our work showed a high current density as compared to the AOR results performed in low temperatures [28–35]. Furthermore, the H₂ production rate was about 1.8 times higher than the hybrid thermal–electrochemical NH₃ conversion to H₂ in the SAEC system without a thermal cracking layer composed of Ru catalysts [14]. These indicated that the SAEC system has a great potential for electrochemical oxidation of NH₃ to H₂ and the performance can be significantly enhanced by moderately modifying electrolytes and catalyst materials with appropriate and effective additives.

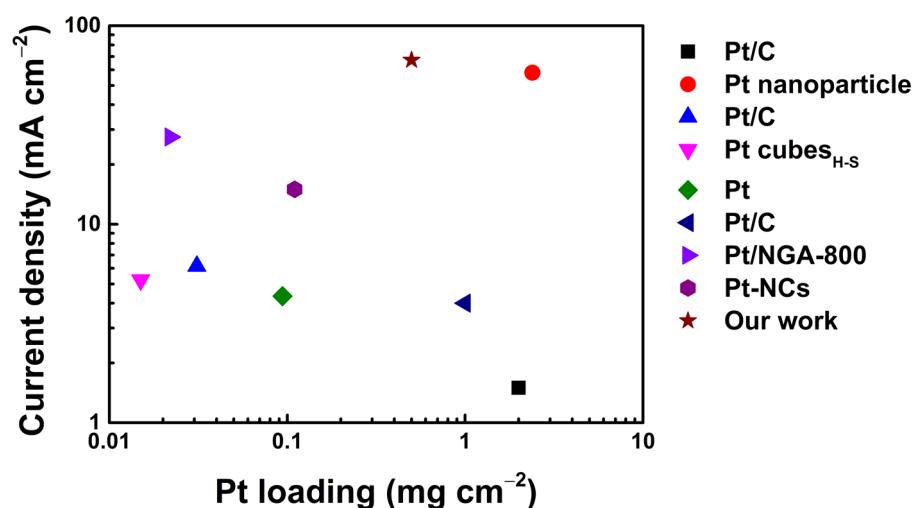


Figure 6. Comparison of AOR current density against Pt loading mass with reported AOR studies at low temperature [28–35].

3. Materials and Methods

3.1. Synthesis of CsH₂PO₄ and SiP₂O₇

For the synthesis of cesium dihydrogen phosphate (CsH₂PO₄) powder, CsCO₃ (99% metal basis, Alfa Aesar, Haverhill, MA, USA), and H₃PO₄ (85 wt% aqueous solution, Alfa Aesar, Haverhill, MA, USA) were mixed in a 1:1 molar ratio in an aqueous solution. Afterwards, methanol was added to the solution, followed by precipitation of CsH₂PO₄. The precipitate was filtered and dried at 80 °C for 12 h. SiP₂O₇ was synthesized by mixing SiO₂ (99.9% 0.5 micron, Alfa Aesar, Haverhill, MA, USA) and H₃PO₄ solution in a 1:2 molar ratio. The mixture was heated at 200 °C for 3 h and at 100 °C for 24 h subsequently. After the heat treatment, the mixture was ground and subsequently heated at 122 °C for 24 h and at 700 °C for 3 h. All heating steps were carried out under air condition, and as-prepared CsH₂PO₄ and SiP₂O₇ were mixed in a 1:2 molar ratio.

3.2. SAEC Cell Preparation

Anode and cathode were prepared by mixing Pt/C (20 wt% of Pt on carbon black, Alfa Aesar, Haverhill, MA, USA), electrolyte composite in 1:3, 1:6, 1:9 weight ratio in toluene (Pt/C_CDP/SPO-3, 6, 9). The resultant solution was loaded on a carbon paper (TGP-H-90, Toray, Tokyo, Japan) to 0.5 mg_{Pt} cm⁻² by drop casting. Then, CsH₂PO₄/SiP₂O₇ suspended

toluene solution was deposited on anode carbon paper and dried at 100 °C to compose the electrolyte layer. In addition, porous stainless steel mesh (Sus 316 150 mesh) was used as both a current collector and mechanical support of the cell. The porous stainless steel mesh, anode paper with electrolyte, cathode paper, and stainless steel mesh were stacked in a steel chamber in a row and pressed at 80 MPa for 5 min to fabricate a solid acid electrolysis cell, and the cell was sealed using PTFE tape.

The gas flow system was illustrated in Figure S7. Ag wires connected to the stainless steel mesh were used as terminals for both electrodes to a potentiostat (VSP-300). The cell was heated from 25 °C to 250 °C for 1 h with a humidified N₂ gas flow of 30 mL min⁻¹ on the cathode side and a humidified Ar gas flow of 30 mL min⁻¹ on the anode side. At 250 °C, the flow of Ar gas was reduced to 15 mL min⁻¹ and humidified NH₃ was supplied together to the anode side. Humidified conditions (30%) of gas flow at each side were achieved by passing through the bubbler at 70 °C.

3.3. Electrochemical Measurements

To evaluate the ammonia oxidation activities of the solid acid cell, the reaction was performed at 250 °C from 0.5 V to 0.8 V at different NH₃ flow rates (20, 40, 60 mL min⁻¹). Electrochemical impedance spectroscopy (EIS) was performed at open circuit voltage (OCV) in the frequency range from 10⁴ Hz to 0.1 Hz. The outlet gas from the cathode was penetrated through a water trap to check the NH₃ crossover from the anode side, and then sampled to gas chromatography (Agilent 7890A, Santa Clara, CA, USA) with a thermal conductivity detector (TCD) to estimate the H₂ gas production rate. The trapped NH₃ was detected by UV-visible spectroscopy (Agilent Technologies Cary 8454, Santa Clara, CA, USA) using the indophenol blue method. The reagent was made by preparing 2 mL of 1 M NaOH solution containing 5 wt% salicylic acid and 5 wt% sodium citrate, followed by addition of 1 mL of 0.05 M NaClO and 0.01 mL of 1 wt% sodium nitroferrocyanide aqueous solution.

3.4. Structural Characterization

The morphology of the electrode material was analyzed through scanning electron microscopy (SEM) data using a JSM 7800F instrument operated at 10 kV. Furthermore, X-ray diffraction (XRD) analysis data were obtained by Ultima IV (Rigaku) using Cu K α ($\lambda = 1.5418 \text{ \AA}$) radiation operated at 40 kV and 30 mA to obtain the crystal structure information of synthesized materials.

4. Conclusions

In summary, we have successfully prepared the electrolyte composite and electrode materials for the SAEC system and applied this to the electrochemical NH₃ oxidation to produce a high-purity H₂ in the intermediate temperatures around 250 °C. The electrolyte composite was prepared by mixing CDP and SPO to enhance the thermal stability and proton conductivity for the broader temperature range, and it was further used to modify the Pt/C catalysts with different ratios to boost the electrocatalytic activity further. The AOR performance using the Pt/C_CDP/SPO-6 as the electrode material achieved a maximum Faradaic efficiency of 98.2% and dihydrogen production rate of 1.33 mmol h⁻¹ cm⁻². Furthermore, in a long-term durability test, it was confirmed that a current density of 7.5 mA cm⁻² was maintained for longer than 20 h with no significant morphological changes. We discovered that a proper mixing ratio of the solid acid electrolyte composites and the Pt/C-based catalyst materials is required to optimize the electrolysis performance of NH₃ over the SAEC. The modified electrolyte and catalyst indicated a higher performance for dihydrogen evolution from electrochemical ammonia decomposition as compared to the previously reported results in low temperatures and the hybrid thermal–electrochemical NH₃ decomposition in the SAEC system. Consequently, this study can give a new approach toward an SAEC that is operable at intermediate temperatures with developments

of efficient electrolytes and active electrode catalysts in the research field of ammonia electrooxidation for dihydrogen production.

Supplementary Materials: The following supporting information can be downloaded at: <https://www.mdpi.com/article/10.3390/catal13040707/s1>, Figure S1: Linear sweep voltammetry (LSV) curves of Pt/C_CDP/SPO-x catalysts for AOR from 0 to 0.8 V at 10 mV s⁻¹ scan rate; Figure S2: GC-TCD analysis of cathode outlet gas for the AOR using the Pt/C_CDP/SPO-6 catalyst at 0.8 V at a flow rate of NH₃ of 60 mL min⁻¹ (a) from 0.8 to 1.2 min and (b) from 1.2 to 15 min; Figure S3: Deactivation rate of the Pt/C_CDP/SPO-6 catalyst at ammonia flow rate of 60 mL min⁻¹ at 0.8 V for 20 h; Figure S4: (a) XRD patterns of the pristine Pt/C_CDP/SPO-6 and after the long-term stability test. (b) SEM images and EDS elemental mapping of Pt, Cs and Si of Pt/C_CDP/SPO-6 after stability test; Figure S5: (a) UV-vis absorption spectra and (b) calibration curve for the indophenol blue method; Figure S6: Comparison of mass activity for AOR over Pt-based catalysts with reported AOR literatures at low temperatures; Figure S7: Schematic illustration of the overall AOR process with the SAEC system; Table S1: Electrochemical impedance parameters of Pt/C_CDP/SPO-x catalysts at open circuit voltage under 60 mL min⁻¹ ammonia flow rate condition; Table S2: Analyses of ammonia crossover during the electrochemical AOR in the SAEC for 60 min. The references [35–42] are cited in the Supplementary Materials.

Author Contributions: Conceptualization, J.K. and H.H.S.; Methodology, J.M.; Formal analysis, J.K.; Investigation, D.J., J.C. and T.P.; Writing—original draft, J.K. and D.J.; Writing—review & editing, W.B.K.; Supervision, W.B.K. All authors have read and agreed to the published version of the manuscript.

Funding: This research was supported by the Basic Science Research Program through the National Research Foundation of Korea (NRF) funded by the Ministry of Science and ICT (NRF-2019R1A2C2088174) and by the “Human Resources Program in Energy Technology” of the Korea Institute of Energy Technology Evaluation and Planning (KETEP), granted financial resource from the Ministry of Trade, Industry & Energy, Republic of Korea (No. 20204010600100), and also by the National Research Foundation of Korea (NRF) grant funded by the Korean Government (MSIT) (No. 2021R1A5A1084921).

Conflicts of Interest: The authors declare no conflict of interest.

References

1. Dyatlov, S.A.; Didenko, N.I.; Ivanova, E.A.; Soshneva, E.B.; Kulik, S.V. Prospects for Alternative Energy Sources in Global Energy Sector. *IOP Conf. Ser. Earth Environ. Sci.* **2020**, *434*, 012014. [[CrossRef](#)]
2. Yan, Y.; Zhang, J.Y.; Shi, X.R.; Zhu, Y.; Xia, C.; Zaman, S.; Hu, X.; Wang, X.; Xia, B.Y. A Zeolitic-Imidazole Framework-Derived Trifunctional Electrocatalyst for Hydrazine Fuel Cells. *ACS Nano* **2021**, *15*, 10286–10295. [[CrossRef](#)]
3. Rivard, E.; Trudeau, M.; Zaghbi, K. Hydrogen Storage for Mobility: A Review. *Materials* **2019**, *12*, 1973. [[CrossRef](#)] [[PubMed](#)]
4. Lee, H.J.; Park, E.D. Ammonia Decomposition over Ru/SiO₂ Catalysts. *Catalysts* **2022**, *12*, 1203. [[CrossRef](#)]
5. Jang, D.; Maeng, J.; Kim, J.; Han, H.; Park, G.H.; Ha, J.; Shin, D.; Hwang, Y.J.; Kim, W.B. Boosting Electrocatalytic Nitrate Reduction Reaction for Ammonia Synthesis by Plasma-Induced Oxygen Vacancies over MnCuOx. *Appl. Surf. Sci.* **2023**, *610*, 155521. [[CrossRef](#)]
6. Lucentini, I.; Garcia, X.; Vendrell, X.; Llorca, J. Review of the Decomposition of Ammonia to Generate Hydrogen. *Ind. Eng. Chem. Res.* **2021**, *60*, 18560–18611. [[CrossRef](#)]
7. Uribe, F.A.; Gottesfeld, S.; Zawodzinski, T.A. Effect of Ammonia as Potential Fuel Impurity on Proton Exchange Membrane Fuel Cell Performance. *J. Electrochem. Soc.* **2002**, *149*, A293. [[CrossRef](#)]
8. Mukherjee, S.; Devaguptapu, S.V.; Sviripa, A.; Lund, C.R.F.; Wu, G. Low-Temperature Ammonia Decomposition Catalysts for Hydrogen Generation. *Appl. Catal. Environ.* **2018**, *226*, 162–181. [[CrossRef](#)]
9. Lamb, K.E.; Dolan, M.D.; Kennedy, D.F. Ammonia for Hydrogen Storage: A Review of Catalytic Ammonia Decomposition and Hydrogen Separation and Purification. *Int. J. Hydrogen Energy* **2019**, *44*, 3580–3593. [[CrossRef](#)]
10. Kim, H.; Hong, S.; Kim, H.; Jun, Y.; Kim, S.Y.; Ahn, S.H. Recent Progress in Pt-Based Electrocatalysts for Ammonia Oxidation Reaction. *Appl. Mater. Today* **2022**, *29*, 101640. [[CrossRef](#)]
11. Haile, S.M.; Boysen, D.A.; Chisholm, C.R.I.; Merle, R.B. Solid acids as fuel cell electrolytes. *Nature* **2001**, *410*, 910–913. [[CrossRef](#)] [[PubMed](#)]
12. Boysen, D.A.; Uda, T.; Chisholm, C.R.I.; Haile, S.M. High-Performance Solid Acid Fuel Cells through Humidity Stabilization. *Science* **2004**, *303*, 68–70. [[CrossRef](#)] [[PubMed](#)]

13. Fujiwara, N.; Nagase, H.; Tada, S.; Kikuchi, R. Hydrogen Production by Steam Electrolysis in Solid Acid Electrolysis Cells. *ChemSusChem* **2021**, *14*, 417–427. [[CrossRef](#)]
14. Taninouchi, Y.-K.; Uda, T.; Awakura, Y.; Ikeda, A.; Haile, S.M. Dehydration behavior of the superprotonic conductor CsH₂PO₄ at moderate temperatures: 230 to 260 °C. *J. Mater. Chem.* **2007**, *17*, 3182–3189. [[CrossRef](#)]
15. Yuan, Y.; Tada, S.; Kikuchi, R. Ammonia Synthesis Using Fe/BZY–RuO₂ Catalysts and a Caesium Dihydrogen Phosphate-Based Electrolyte at Intermediate Temperatures. *Mater. Adv.* **2021**, *2*, 793–803. [[CrossRef](#)]
16. Kishira, S.; Qing, G.; Suzu, S.; Kikuchi, R.; Takagaki, A.; Oyama, S.T. Ammonia Synthesis at Intermediate Temperatures in Solid-State Electrochemical Cells Using Cesium Hydrogen Phosphate Based Electrolytes and Noble Metal Catalysts. *Int. J. Hydrogen Energy* **2017**, *42*, 26843–26854. [[CrossRef](#)]
17. Imamura, K.; Kubota, J. Ammonia Synthesis from Nitrogen and Water at Intermediate Temperatures and Elevated Pressures by Using an Electrochemical Hydrogen-Membrane Reactor with Supported Ru Catalysts and Phosphate Electrolytes. *Sustain. Energy Fuels* **2019**, *3*, 1406–1417. [[CrossRef](#)]
18. Lim, D.K.; Plymill, A.B.; Paik, H.; Qian, X.; Zecevic, S.; Chisholm, C.R.I.; Haile, S.M. Solid Acid Electrochemical Cell for the Production of Hydrogen from Ammonia. *Joule* **2020**, *4*, 2338–2347. [[CrossRef](#)]
19. Matsui, T.; Kukino, T.; Kikuchi, R.; Eguchi, K. An Intermediate Temperature Proton-Conducting Electrolyte Based on a CsH₂PO₄/SiP₂O₇ Composite. *Electrochim. Solid-State Lett.* **2005**, *8*, 256–259. [[CrossRef](#)]
20. Dogu, D.; Gunduz, S.; Meyer, K.E.; Deka, D.J.; Co, A.C.; Ozkan, U.S. CO₂ and H₂O Electrolysis Using Solid Oxide Electrolyzer Cell (SOEC) with La and Cl-doped Strontium Titanate Cathode. *Catal. Lett.* **2019**, *149*, 1743–3752. [[CrossRef](#)]
21. Adli, N.M.; Zhang, H.; Mukherjee, S.; Wu, G. Review—Ammonia Oxidation Electrocatalysis for Hydrogen Generation and Fuel Cells. *J. Electrochem. Soc.* **2018**, *165*, J3130–J3147. [[CrossRef](#)]
22. Pillai, H.S.; Xin, H. New Insights into Electrochemical Ammonia Oxidation on Pt(100) from First Principles. *Ind. Eng. Chem. Res.* **2019**, *58*, 10819–10828. [[CrossRef](#)]
23. Franceschini, E.A.; Lacconi, G.I.; Corti, H.R. Hydrogen evolution kinetics on Ni cathodes modified by spontaneous deposition of Ag or Cu. *J. Energy. Chem.* **2017**, *26*, 466–475. [[CrossRef](#)]
24. Xiong, W.; Guo, Z.; Zhao, S.; Wang, Q.; Xu, Q.; Wang, X. Facile, Cost-Effective Plasma Synthesis of Self-Supportive FeS: X on Fe Foam for Efficient Electrochemical Reduction of N₂ under Ambient Conditions. *J. Mater. Chem.* **2019**, *7*, 19977–19983. [[CrossRef](#)]
25. Li, W.; Li, K.; Ye, Y.; Zhang, S.; Liu, Y.; Wang, G.; Liang, C.; Zhang, H.; Zhao, H. Efficient Electrocatalytic Nitrogen Reduction to Ammonia with Aqueous Silver Nanodots. *Commun. Chem.* **2021**, *4*, 10. [[CrossRef](#)]
26. Miyaoka, H.; Miyaoka, H.; Ichikawa, T.; Ichikawa, T.; Kojima, Y. Highly Purified Hydrogen Production from Ammonia for PEM Fuel Cell. *Int. J. Hydrogen Energy* **2018**, *43*, 14486–14492. [[CrossRef](#)]
27. Dushina, A.; Schonvogel, D.; Fischer, Y.; Büselmann, J.; Dyck, A.; Wagner, P. Influence of Ammonia Contamination on HT-PEM Fuel Cell Platinum Catalyst. *ECS Trans.* **2020**, *98*, 537–552. [[CrossRef](#)]
28. Zhao, Y.; Setzler, B.P.; Wang, J.; Nash, J.; Wang, T.; Xu, B.; Yan, Y. An Efficient Direct Ammonia Fuel Cell for Affordable Carbon-Neutral Transportation. *Joule* **2019**, *3*, 2472–2484. [[CrossRef](#)]
29. Hanada, N.; Kohase, Y.; Hori, K.; Sugime, H.; Noda, S. Electrolysis of ammonia in aqueous solution by platinum nanoparticles supported on carbon nanotube film electrode. *Electrochim. Acta* **2020**, *341*, 136027. [[CrossRef](#)]
30. Li, Z.-F.; Wang, Y.; Botte, G.G. Revisiting the electrochemical oxidation of ammonia on carbon-supported metal nanoparticle catalysts. *Electrochim. Acta* **2017**, *228*, 351–360. [[CrossRef](#)]
31. Jin, H.; Lee, S.; Sohn, Y.; Lee, S.-H.; Kim, P.; Yoo, S.J. Capping agent-free synthesis of surface engineered Pt nanocube for direct ammonia fuel cell. *Int. J. Energy Res.* **2021**, *45*, 18281–18291. [[CrossRef](#)]
32. Liu, J.; Hu, W.; Zhong, C.; Cheng, Y.F. Surfactant-free electrochemical synthesis of hierarchical platinum particle electrocatalysts for oxidation of ammonia. *J. Power Sources* **2013**, *223*, 165–174. [[CrossRef](#)]
33. Gwak, J.; Choun, M.; Lee, J. Alkaline ammonia electrolysis on electrodeposited platinum for controllable hydrogen production. *ChemSusChem* **2016**, *9*, 403–408. [[CrossRef](#)]
34. Zhou, Y.; Zhang, G.; Yu, M.; Wang, X.; Lv, J.; Yang, F. Free-Standing 3D Porous N-Doped Graphene Aerogel Supported Platinum Nanocluster for Efficient Hydrogen Production from Ammonia Electrolysis. *ACS Sustain. Chem. Eng.* **2018**, *6*, 8437–8446. [[CrossRef](#)]
35. Sun, H.-Y.; Xu, G.-R.; Li, F.-M.; Hong, Q.-L.; Jin, P.-J.; Chen, P.; Chen, Y. Hydrogen generation from ammonia electrolysis on bifunctional platinum nanocubes electrocatalysts. *J. Energy Chem.* **2020**, *47*, 234–240. [[CrossRef](#)]
36. Song, L.; Liang, Z.; Ma, Z.; Zhang, Y.; Chen, J.; Adzic, R.R.; Wang, J.X. Temperature-Dependent Kinetics and Reaction Mechanism of Ammonia Oxidation on Pt, Ir, and PtIr Alloy Catalysts. *J. Electrochem. Soc.* **2018**, *165*, J3095–J3100. [[CrossRef](#)]
37. Li, S.; Chen, H.; Liu, J.; Deng, Y.; Han, X.; Hu, W.; Zhong, C. Size- and Density-Controllable Fabrication of the Platinum Nanoparticle/ITO Electrode by Pulse Potential Electrodeposition for Ammonia Oxidation. *ACS Appl. Mater. Interface* **2017**, *9*, 27765–27772. [[CrossRef](#)] [[PubMed](#)]
38. Zhou, Y.F.; Zhang, G.Q.; Gong, Z.; Shang, X.L.; Yang, F.L. Potentiodynamic Uniform Anchoring of Platinum Nanoparticles on N-Doped Graphene with Improved Mass Activity for the Electrooxidation of Ammonia. *ChemElectroChem* **2016**, *3*, 605–614. [[CrossRef](#)]
39. Kang, Y.; Wang, W.; Li, J.; Li, Q.; Liu, S.; Lei, Z. A Highly Efficient Pt-NiO/C Electrocatalyst for Ammonia Electro-Oxidation. *J. Electrochem. Soc.* **2017**, *164*, F958–F965. [[CrossRef](#)]

40. Ntais, S.; Serov, A.; Andersen, N.I.; Roy, A.J.; Cossar, E.; Allagui, A.; Lu, Z.Z.; Cui, X.Y.; Baranova, E.A.; Atanasov, P. Promotion of Ammonia Electrooxidation on Pt nanoparticles by Nickel Oxide Support. *Electrochim. Acta* **2016**, *222*, 1455–1463. [[CrossRef](#)]
41. Liu, J.; Chen, B.; Kou, Y.; Liu, Z.; Chen, X.; Li, Y.; Deng, Y.; Han, X.; Hu, W.; Zhong, C. Pt-Decorated highly porous flower-like Ni particles with high mass activity for ammonia electro-oxidation. *J. Mater. Chem.* **2016**, *4*, 11060–11068. [[CrossRef](#)]
42. Du, X.T.; Yang, Y.; Liu, J.; Liu, B.; Liu, J.B.; Zhong, C.; Hu, W.B. Surfactant-free and template-free electrochemical approach to prepare well-dispersed Pt nanosheets and their high electrocatalytic activities for ammonia oxidation. *Electrochim. Acta* **2013**, *111*, 562–566. [[CrossRef](#)]

Disclaimer/Publisher's Note: The statements, opinions and data contained in all publications are solely those of the individual author(s) and contributor(s) and not of MDPI and/or the editor(s). MDPI and/or the editor(s) disclaim responsibility for any injury to people or property resulting from any ideas, methods, instructions or products referred to in the content.